IOP Publishing Superconductor Science and Technology
Supercond. Sci. Technol. **28** (2015) 045008 (12pp) doi:10.1088/0953-2048/28/4/045008

# Direct-current superconducting quantum interference devices for the readout of metallic magnetic calorimeters

**S Kempf, A Ferring, A Fleischmann and C Enss**

Kirchhoff-Institute for Physics, Heidelberg University, Im Neuenheimer Feld 227, D-69120 Heidelberg, Germany

E-mail: sebastian.kempf@kip.uni-heidelberg.de

Received 10 December 2014, revised 20 January 2015
Accepted for publication 26 January 2015
Published 12 February 2015

**Abstract**

In this paper we analyze the influence of the coupled energy sensitivity $\epsilon_c(f)$ of a superconducting quantum interference device (SQUID) on the energy resolution of metallic magnetic calorimeters. From this, we derive an upper limit on the readout noise that still allows for the readout of detectors with sub-eV energy resolution. Furthermore, we present two dc-SQUID designs, namely a first-stage SQUID and an *N*-SQUID series array, that are suited for the readout of high-resolution detectors. We show that fabricated SQUIDs have a noise performance that is competitive to the best state-of-the-art dc-SQUIDs. For the first-stage SQUIDs, we found a correlation between the $1/f$ noise exponent $\alpha$ and the $1/f$ noise prefactor $\epsilon_{1/f}$ (1 Hz). Using both kind of SQUIDs we have built a two-stage dc-SQUID configuration. We show that this setup allows for the readout of x-ray detectors with a resolving power $E/\Delta E_{\mathrm{FWHM}} > 3000$.

Keywords: metallic magnetic calorimeters, direct-current superconducting quantum interference devices, $1/f$ noise, low-temperature microcalorimeters, SQUID design

(Some figures may appear in colour only in the online journal)

## 1. Introduction

Superconducting quantum interference devices (SQUIDs) are presently the most sensitive wideband devices for measuring quantities that can be naturally converted into magnetic flux [1]. Along with their compatibility with mK operation temperatures they are particularly well suited for the readout of calorimetric low-temperature particle detectors (LTDs) such as superconducting transition edge sensors [2], magnetic penetration thermometers [3] and metallic magnetic calorimeters (MMCs) [4]. In general, an LTD consists of an absorber for the particles to be detected that is in tight thermal contact to a sensitive thermometer monitoring the temperature change of the detector upon the absorption of an energetic particle. In case of MMCs a paramagnetic temperature sensor that is situated in a weak magnetic field converts the temperature rise into a change of sensor magnetization. For single-channel detectors as well as small-scale detector arrays this magnetization change is mostly measured with current-sensing dc-SQUIDs monitoring the current through a superconducting pickup coil that is placed in close proximity to the temperature sensor [4, 5].

Very recently, MMCs have reached an energy resolving power $E/\Delta E_{\mathrm{FWHM}} > 3500$, i.e. an energy resolution $\Delta E_{\mathrm{FWHM}} = 1.6$ eV for x-rays with energies $E$ up to 6 keV [6]. However, the energy resolution of MMCs has still not reached the fundamental limit which is set by thermodynamic energy fluctuations between the detector and the thermal bath as well as between the spin and electron system within the detector [3, 4]. Among other things, one reason is that the performance of MMCs depends on the properties of the SQUID that is used for detector readout. In particular, it is known that SQUID noise can significantly affect the overall signal-to-noise ratio of non-optimized detector configurations and often set a limit to the energy resolution [3–5]. But since the responsitivity of MMCs can be calculated with confidence and all relevant noise contributions can be modeled very well [4, 5, 7], MMCs can be optimized with respect to the energy

 

resolution [4, 5]. Moreover, the predictability of the signal size and the overall noise spectrum allows for the development of SQUIDs that are specifically optimized for MMC readout, e.g. in terms of input coil inductance.

The readout of MMCs with sub-eV energy resolution requires a SQUID with a coupled energy sensitivity $\epsilon_{c,w} < 15\,h$ in the white noise region and an $1/f$ corner frequency $f_c < 200$ Hz as will be shown in section 2. Furthermore, the system bandwidth needs to be larger than 1 MHz to resolve the fast signal rise time of MMCs that can be as low as 70 ns [5, 8]. To provide both, a low energy sensitivity $\epsilon_c(f)$ and a large system bandwidth, two dc-SQUIDs are often arranged in a two-stage SQUID configuration [9]. Here, the output signal of the first-stage SQUID to which the detector is connected to is coupled into the input of a second-stage SQUID, e.g. an *N*-SQUID series array, acting as a low noise amplifier. To linearize the SQUID response and therefore to increase its dynamic range, a flux-locked loop (FLL) to the first-stage SQUID is typically used [9]. For sufficient high flux gain between the first- and second-stage SQUID, the effects of amplifier SQUID and room-temperature electronics preamplifier noise are greatly suppressed. This allows for low-noise direct SQUID readout with a large closed-loop system bandwidth of up to some 100 MHz [10].

## 2. Influence of readout noise on the energy resolution of MMCs

The energy resolution $\Delta E_{FWHM}$ of MMCs is mainly determined by four different noise contributions [4]. These are (i) thermodynamic energy fluctuations between the detector and the thermal bath as well as between the spin and electron system, (ii) magnetic Johnson noise due to the Brownian motion of electrons within metallic detector components, (iii) an $1/f$ like noise contribution that has been observed in all state-of-the-art MMCs employing Au:Er temperature sensors [5] and (iv) SQUID readout noise. The latter is addressed within this paper and is commonly expressed by the coupled energy sensitivity $\epsilon_c(f)$ that is referred to the SQUID input coil. Typically, $\epsilon_c(f)$ is composed of a white noise contribution $\epsilon_{c,w}$ and a frequency dependent contribution $\epsilon_{c,1/f} \propto f^{-\alpha}$ with $\alpha = 0.5\ldots1$ [11] which we will hereinafter denote as $1/f$ noise even if the exponent $\alpha$ differs from 1.

The signal size as well as the absolute values of the noise contributions and therefore the energy resolution $\Delta E_{FWHM}$ depend on a number of parameters that either are fixed by experimental boundary conditions or that can be freely varied within a certain parameter range. Typically, the operation temperature $T$ is fixed and the lateral size of the detector as well as the quantum efficiency for the particles to be detected are specified by the application the detector is developed for. The absorber heat capacity $C_{abs}$ is then fixed by the choice of an absorber material. In contrast, the magnetic field generating persistent current $I_0$ running inside the pickup coil as well as the area $A_s$, the height $h_s$ and the erbium concentration $x_{Er}$ of the temperature sensor can be varied over wide ranges.

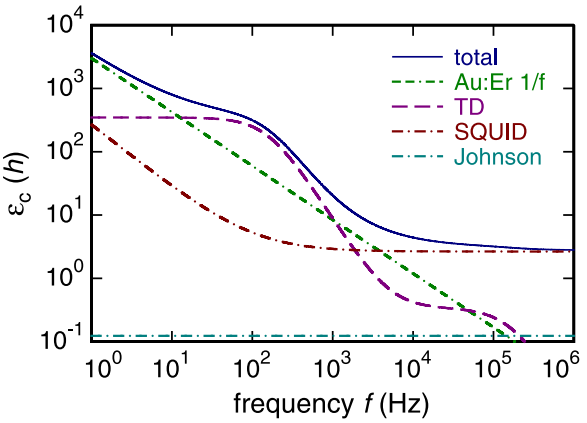


**Figure 1.** Calculated coupled energy sensitivity $\epsilon_c$ versus frequency $f$ for an optimized detector with meander-shaped pickup coil and Au:Er temperature sensor. The detector is assumed to be read out by a SQUID with a coupled energy sensitivity $\epsilon_{c,w} = 2\,h$ in the white noise region and a corner frequency $f_c = 100$ Hz of true $1/f$ noise. Dashed lines represents different noise contributions where the contribution of the thermodynamic energy fluctuations is denoted as TD.

To investigate the influence of the readout noise on the energy resolution we want to consider a state-of-the-art x-ray detector with a single Au:Er temperature sensor and a meander-shaped pickup coil with 3 $\mu$m linewidth and 6 $\mu$m pitch and optimize this detector for a given energy sensitivity $\epsilon_c(f)$ with respect to the energy resolution. For this, we assume the detector to have an absorber heat capacity of $C_{abs} = 0.15\,\mathrm{pJ\,K^{-1}}$ at an operation temperature of $T = 30$ mK. The rise time $\tau_0$ and the decay time $\tau_1$ of the detector are chosen to be 1 $\mu$s and 1 ms, respectively. Furthermore, we assume that the input coil of the SQUID is wire-bonded to the pickup coil of the detector with superconducting bonding wires with an inductance $L_w = 500$ pH. Within our calculations we suppose that the input coil inductance $L_{in}$ of the SQUID is a free parameter that can be varied within a certain parameter range while maintaining a constant magnetic coupling factor $k_{in}$ between the SQUID loop and the input coil.

For detector optimization, we preset an energy sensitivity $\epsilon_c(f)$ of the SQUID readout and numerically calculate the detector response as well as the overall noise spectrum for a large number of parameter sets ($A_s$, $h_s$, $x_{Er}$, $I_0$, $L_{in}$). We then numerically calculate the energy resolution for each parameter set within the framework of optimal filtering [12]. To determine the energy resolution $\Delta E_{FWHM}$ of the detector, we search for the global minimum in this multi-dimensional parameter space.

Figure 1 shows the calculated coupled energy sensitivity $\epsilon_c(f)$ as well as the contributions of the different noise sources referred to the input coil of the SQUID versus frequency $f$ for an optimized detector as discussed above. The detector is assumed to be read out by a SQUID with a coupled energy sensitivity $\epsilon_{c,w} = 2\,h$ in the white noise region and a corner frequency $f_c = 100$ Hz of true $1/f$ noise. It is clearly visible that the white noise contribution of the SQUID dominates the overall noise spectrum for frequencies $f > 3.4$ kHz and is

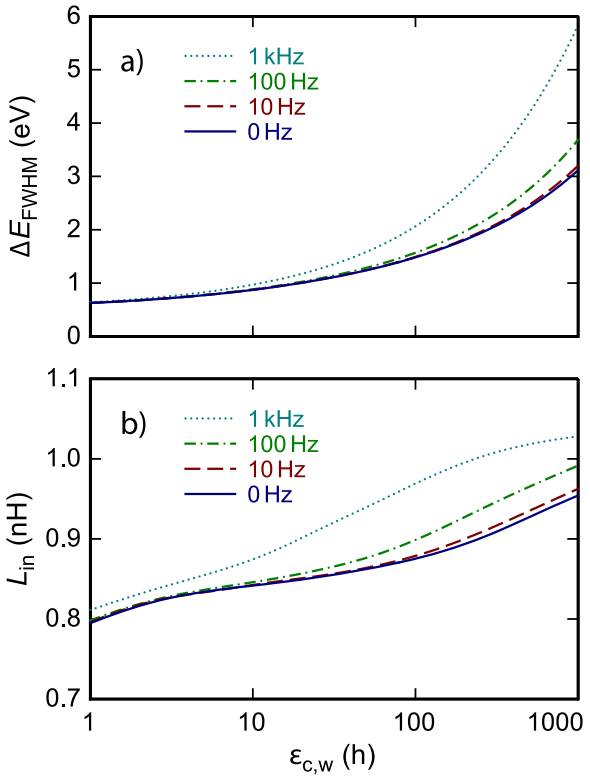


**Figure 2.** (a) Energy resolution $\Delta E_{\mathrm{FWHM}}$ and (b) optimum value of the SQUID input coil inductance $L_{\mathrm{in}}$ of an optimized detector with meander-shaped pickup coil and Au:Er temperature sensor versus the white noise contribution $\epsilon_{\mathrm{c,w}}$ of the energy sensitivity of the SQUID readout for different values of the $1/f$ corner frequency $f_{\mathrm{c}}$.

roughly one order of magnitude larger than the high frequency plateau of the thermodynamic energy fluctuations. It therefore sets a limit to the overall signal-to-noise ratio and thus to the energy resolution of the detector. For frequencies $f < 10$ Hz, the overall noise spectrum is dominated by the $1/f$ noise contribution attributed to the Er ions within the temperature sensor. Concerning the noise performance, this makes small erbium concentrations $x_{\mathrm{Er}}$ more favorable. However, the signal size as well as the absolute values of the thermodynamic energy fluctuations plateaus gets smaller as the Er concentration is lowered. This makes the influence of the SQUID white noise on the overall noise spectrum and therefore on the energy resolution more pronounced. The optimum Er concentration needs hence to be a compromise between the degradation of the energy resolution due to the $1/f$ noise contribution of the Er ions and the influence of the SQUID readout noise on the overall noise spectrum.

Figure 2 shows that the energy resolution $\Delta E_{\mathrm{FWHM}}$ of an optimized detector strongly increases with the coupled energy sensitivity $\epsilon_{\mathrm{c}}(f)$ of the SQUID readout. But since this degradation of $\Delta E_{\mathrm{FWHM}}$ can be partially compensated by higher Er concentrations and larger sensor volumes this increase still allows for detectors with sub-eV energy resolution in case of a SQUID readout with $\epsilon_{\mathrm{c,w}} < 10\,h$. However, the energy resolution is deteriorated by more than 50% compared to an ideal readout with $\epsilon_{\mathrm{c,w}} \to 0$. For $\epsilon_{\mathrm{c,w}} > 10\,h$, the noise contribution of the SQUID readout can hardly be compensated because the influence of the $1/f$ noise contribution attributed to the Er ions increases more strongly than the signal size. This leads to an even stronger influence of the noise contribution of the SQUID readout on the energy resolution. For a SQUID readout with $\epsilon_{\mathrm{c,w}} \gg 1000\,h$ the overall noise spectrum is fully dominated by the SQUID readout. The energy resolution therefore rapidly increases with $\epsilon_{\mathrm{c,w}}$ and can be more than order of magnitude larger than the intrinsic detector energy resolution.

Our simulations also verify that an important requirement for high-resolution detectors is inductance matching between detector and SQUID. More precisely, optimum flux coupling between detector and SQUID is achieved for $L_{\mathrm{in}} = L_{\mathrm{w}} + L_{\mathrm{p}}$, i.e. the input coil inductance $L_{\mathrm{in}}$ of the SQUID matches the sum of the parasitic inductance $L_{\mathrm{w}}$ within the flux transformer and the inductance $L_{\mathrm{p}}$ of the pickup coil. For $L_{\mathrm{w}} = 500$ pH which is a realistic value according to our experience the input coil inductance $L_{\mathrm{in}}$ should be in the range between 800 pH and 1.1 nH (see figure 2).

In summary, the readout of MMCs with sub-eV energy resolution requires a SQUID readout with a coupled energy sensitivity $\epsilon_{\mathrm{c,w}} < 15\,h$ in the white noise region, an $1/f$ corner frequency $f_{\mathrm{c}} < 200$ Hz and a SQUID input coil inductance of about 900 pH assuming realistic values for stray inductances within the flux transformer.

## 3. SQUID designs

We have developed two dc-SQUID designs, namely a first-stage SQUID and an *N*-SQUID series array, that are based on the SQUID designs discussed in [13, 14]. They are intended for operation at mK temperatures and are a first step towards the development of high-resolution MMCs with on-chip dc-SQUID readout which is a suitable possibility for minimizing stray inductances within the flux transformer of the detector. Here, the minimization is simply achieved by avoiding bonding wires and should help to further increase the energy resolving power of MMCs.

### 3.1. First-stage SQUID

Figures 3(a) and (b) show a schematic and an optical microscope picture of the first-stage SQUID to which a detector is supposed to be connected to. It is a second-order parallel thin-film gradiometer that is formed by four rectangular washers with a linewidth of 30 $\mu$m and a washer hole size of 60 $\mu$m. On top of the washers which are electrically insulated by an dielectric layer, an input coil with 1.5 turns per washer and a feedback coil with 0.5 turns per washer are running. They are formed by 5 $\mu$m wide Nb lines that are wound such that the polarity of the flux coupled into the SQUID matches the polarity of each washer. The SQUID inductance $L_{\mathrm{s}}$ as well as the inductances $L_{\mathrm{in}}$ of the input and $L_{\mathrm{fb}}$ of the feedback coil and the corresponding mutual inductances $M_{\mathrm{in}} = k_{\mathrm{in}}(L_{\mathrm{s}}L_{\mathrm{in}})^{1/2}$ and $M_{\mathrm{fb}} = k_{\mathrm{fb}}(L_{\mathrm{s}}L_{\mathrm{fb}})^{1/2}$ of these coils to the SQUID loop were numerically calculated by using InductEx [16] and FastHenry [17]. Assuming a

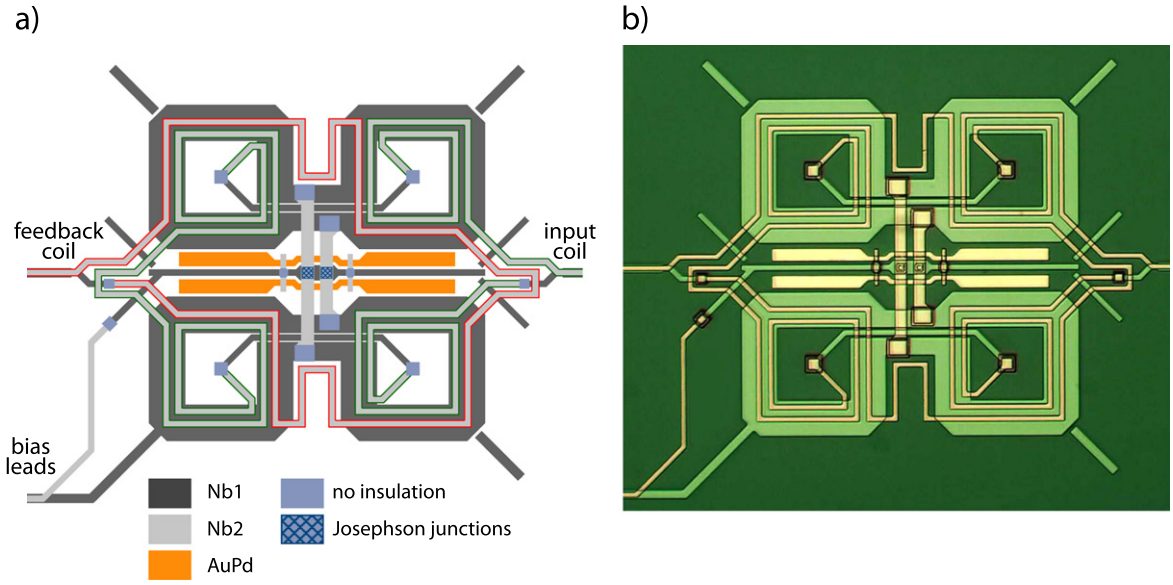


**Figure 3.** (a) Schematic and (b) optical microscope picture of the first-stage SQUID with an input coil and a feedback coil.

penetration depth of 90 nm for Nb at 4.2 K, they are calculated to be $L_s \simeq 45$ pH, $L_{in} \simeq 1.8\,nH$, $L_{fb} \simeq 675$ pH, $M_{in} \simeq 162$ pH and $M_{fb} \simeq 56$ pH, respectively. Since the SQUID design has not yet been optimized in terms of magnetic coupling between the input and feedback coil to the SQUID inductance, i.e. rather large segments of the coils do effectively not couple flux into the SQUID, the magnetic coupling factors takes only values of $k_{in} = 0.57$ and $k_{fb} = 0.32$, respectively.

The SQUID loop is interrupted by two square Josephson junctions with a junction area of $8.5 \times 8.5\,\mu m^2$. They are located in the middle of the SQUID. For a critical current density $j_c = 300\ Acm^{-2}$ at $T < 1\ K$, the critical current $I_0$ of the Josephson junctions is 21.7 $\mu$A. This results in a screening parameter $\beta_L = 2L_sI_0/\Phi_0 \simeq 0.94$ at mK temperatures which is close to the optimum value $\beta_L \simeq 1$ [18]. Both junctions are shunted by two 5 $\mu$m wide and 14 $\mu$m long shunt resistors that are connected in parallel to the junction. Assuming a sheet resistance of 2 $\Omega/\square$ this leads to an effective shunt resistance $R_s = 2.8\ \Omega$ for each junction. The specific capacitance of our Josephson junctions were previously estimated from the frequency of the fundamental SQUID resonance of former devices to be about 18.7 $fF\mu m^{-2}$. Altogether, this results in a hysteresis parameter $\beta_c = 2\pi R^2 CI_0/\Phi_0 \simeq 0.7$ at mK temperatures. Although the ultimate performance of a dc-SQUID is achieved for $\beta_c \simeq 1$ [18], we have chosen a smaller $\beta_c$ in order to ensure stable SQUID operation even if the junction parameters turns out to be slightly larger than expected.

In parallel to the SQUID washers, two 5 $\mu$m wide and 5 $\mu$m long shunt resistors with a design resistance of 2 $\Omega$ are used for properly damping of the fundamental SQUID resonance. To minimize the hot-electron effect [19], the junction shunts as well as the washer shunts are electrically connected to cooling-fins. The bias current is symmetrically injected into the SQUID. To enhance the gradiometry of the SQUID, dummy Nb structures are placed so that local disturbances of background magnetic fields due to neighboring superconducting structures are greatly reduced. For on-chip wiring, in particular for the connection of the input coil to the bonding pads, striplines are used to minimize on-chip parasitic inductances.

### 3.2. N-SQUID series arrays

Figures 4(a) and (b) shows a schematic and an optical microscope picture of a single SQUID cell of our *N*-SQUID series arrays. Each SQUID cell is a first-order series thin-film gradiometer that is formed by two rectangular washers with a linewidth of 7.5 $\mu$m and a washer hole size of 40 $\mu$m. On top of both washers which are electrically insulated by a dielectric layer, two planar coils are running. They are formed by 5 $\mu$m wide Nb lines that are wound such that the polarity of the flux coupled into the SQUID matches the polarity of each washer. On both sides of the array the coils are connected to each other such that they form a single input coil coherently coupling flux into the SQUID. For a single SQUID cell, the SQUID inductance $L_{s,cell}$ and the fraction of the inductance $L_{in,cell}$ of the input coil were numerically calculated to be $L_{s,cell} \simeq 188$ pH and $L_{in,cell} \simeq 216$ pH assuming a penetration depth of 90 nm for Nb at 4.2 K. The connections of the input coil at both sides of the array have in total a parasitic inductance of 20 pH. The mutual inductance $M_{in} = k_{in}(L_{s,cell}L_{in,cell})^{1/2}$ between the input coil and inductance of a single SQUID loop was calculated to be $M_{in} \simeq 150$ pH.

Each SQUID loop is interrupted by two square Josephson junctions with a junction area of $6 \times 6\,\mu m^2$. They are located on the right side of each SQUID cell (see figure 4). For a critical current density of $j_c = 150\ Acm^{-2}$ at mK temperatures, the critical current $I_0$ of the Josephson junctions is 5.4 $\mu$A. This results in a screening parameter $\beta_L = 2L_sI_0/\Phi_0 \simeq 1$ at $T < 1$ K which is close to the optimum value. To avoid hysteretic behavior, each junction is shunted

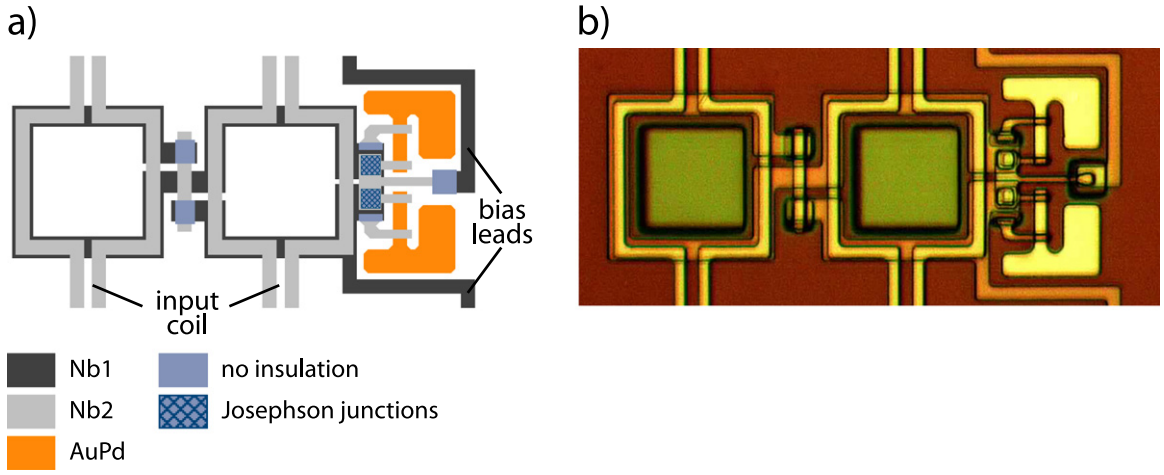


**Figure 4.** (a) Schematic and (b) optical microscope picture of a single SQUID cell of an *N*-SQUID series array with a common input and feedback coil.

by a 5 $\mu$m wide and 10 $\mu$m long shunt resistor that is connected to a cooling fin to minimize the hot electron effect. Assuming a sheet resistance of 2 $\Omega/\square$ this leads to a shunt resistance $R_s = 4\ \Omega$ for each junction. Taking into account the specific capacitance of our Josephson junctions the hysteresis parameter $\beta_c$ takes a value of $\beta_c = 0.18$. Again, we have chosen $\beta_c < 1$ in order to ensure stable SQUID operation even if the junction parameters turn out to be larger than expected.

The bias current is asymmetrically injected into the SQUID cells to enhance the current-to-flux transfer coefficient $I_\Phi$ at the positive slope of the $V$–$\Phi$-characteristic to provide bias current feedback [20]. We have targeted that the contribution of the voltage and current noise of the SQUID electronics are of the same magnitude. For our SQUID arrays we have not placed dummy Nb structures around the SQUID to reduce local disturbances of background magnetic fields and therefore to enhance the gradiometry of the SQUID. However, recent measurements indicate that such dummy structures might be required in future to allow for cooling of the arrays inside the Earth's magnetic field without the need for an elaborate magnetic shielding. For on-chip wiring, in particular for the connection of the input coil to the bonding pads, striplines are used to minimize on-chip parasitic inductances.

## 4. SQUID fabrication

The SQUIDs have been fabricated by using our anodization-free fabrication process for high-quality Nb/Al-$AlO_x$/Nb Josephson junctions which is described in detail in [21]. Therefore we only summarize the most important process steps and outline some modifications that were used for dc-SQUID fabrication.

The fabrication starts with the deposition of a Nb/Al-$AlO_x$/Nb trilayer on a thermally oxidized 2″ Si substrate. The thicknesses of the Nb base electrode and the Nb counter electrode are 250 and 125 nm, respectively. The Al layer that is used for tunnel barrier formation is 18 nm thick. The tunnel barrier is formed by thermal oxidation of the Al layer in a static $O_2$ atmosphere in the load lock of the sputtering system that is used for trilayer deposition. The trilayer critical current density $j_c$ is varied for different batches and is either 150 or 300 $\mathrm{Acm^{-2}}$ for $T < 1\ K$. After trilayer deposition the shape of the counter electrode determining the junction size is patterned by using UV photolithography and inductively coupled plasma reactive ion etching (ICP-RIE) in an $SF_6$ atmosphere. The Al layer is wet-chemically etched. The base electrode is patterned by using UV lithography and ICP-RIE in an $SF_6$ atmosphere. Two $SiO_x$ layers, 430 and 130 nm thick, are used for electrical insulation of the base electrode as well as the sidewalls of the counter electrode. Due to an insufficient thickness calibration of our insulation layers which was recognized only upon completion of different batches including the SQUIDs, these layers are about a factor of 2 thicker than originally foreseen in the design. This results in a reduction of the magnetic coupling factor between the input circuitry and the SQUID loops. On top of the $SiO_x$ layers, AuPd shunt resistors are deposited. For this, a AuPd layer that is patterned by using a lift-off technique is dc magnetron sputtered with a deposition rate of about 9 $\mathrm{Ås^{-1}}$ in an Ar atmosphere at a pressure of 1.3 Pa using a sputter power of 100 W. The thickness of this layer is varied for different batches and ranges from 160 to 320 nm resulting in sheet resistances $R_\square$ ranging from 2 to 1 $\Omega/\square$. The shunt resistors are electrically connected by depositing a 500 nm thick Nb wiring layer that defines also the input and feedback coils, some of the contact pads as wells as SQUID interconnections.

All metal layers including the Nb/Al-$AlO_x$/Nb trilayer are dc magnetron sputtered in a cryo-pumped UHV sputtering system with six sputter guns. The base pressure of the system is below $5 \times 10^{-9}$ mbar. One of the sputter guns is equipped with a Au:$Er_{850\ \mathrm{ppm}}$ sputter target that is routinely used for co-sputtering of paramagnetic temperature sensors during MMC fabrication. As we will see later we have no indications that producing SQUIDs in a sputtering unit that routinely processes paramagnetic materials has any significant influence on

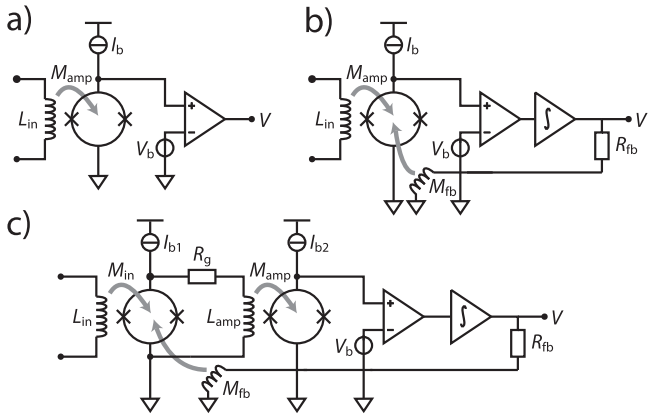


**Figure 5.** Schematics describing the SQUID system in the different proposed configurations: (a) single-stage configuration without FLL (open-loop), (b) single-stage configuration with FLL and (c) two-stage SQUID configuration with FLL to the first-stage SQUID. The SQUID in (a) and (b) might be either a first-stage SQUID or an *N*-SQUID series array.

the low-frequency SQUID noise, contrary to the fact that surface spins are suggested as cause for the low-frequency excess noise (see e.g. [15]).

Up to now, we have fabricated four different batches that are labeled with w01 to w04. The critical current density $j_c$ is 300 $Acm^{-2}$ for batch w01 and 150 $Acm^{-2}$ for batches w02 to w04. The sheet resistances of the AuPd layer are 1 $\Omega/\square$ for w01, 2 $\Omega/\square$ for w02, 1.8 $\Omega/\square$ for w03, and 1.6 $\Omega/\square$ for w04.

## 5. Experimental setup

Fabricated SQUIDs were characterized by using direct SQUID readout with the low-noise and high-bandwidth SQUID electronics XXF-1 from Magnicon GmbH [13]. The first-stage SQUIDs were operated either with a current bias in a single-stage setup (figures 5(a) and (b)) or with a voltage bias in a two-stage configuration (figure 5(c)) for which series SQUID arrays with either 90 or 200 m$\Omega$ on-chip gain resistors were used as a second stage. These arrays were provided by Physikalisch-Technische Bundesanstalt (PTB) Berlin. The *N*-SQUID series arrays were always characterized with a current bias in a single-stage configuration (figures 5(a) and (b)). A basic characterization of the SQUIDs was performed at 4.2 K. For this, the SQUIDs were glued on customized printed circuit boards and mounted into a liquid helium dip probe that is equipped with a home-made soft magnetic cryoperm shield. Low temperature measurements were performed in a dilution refrigerator with a base temperature of about 20 mK . For this, each SQUID was glued onto a Cu holder that was thermally anchored to the mixing chamber and that was surrounded by a superconducting metal shield. The SQUID arrays were in addition shielded by a home-made soft magnetic cryoperm shield.

Basic SQUID characteristics were recorded by running the SQUID electronics in open-loop mode (figure 5(a)) in which the SQUID electronics behaves as an amplifier with very low noise. For determination of characteristic SQUID parameters such as the flux-to-voltage transfer coefficient $V_\Phi$ or the current-to-voltage transfer coefficient $I_\Phi$, the SQUIDs were operated with an FLL (figure 5(b)). Small well-known rectangular test signals were superimposed to the static SQUID biases and the magnetic flux that was fed back into the SQUID was calculated using the voltage output signal of the SQUID electronics, the value of the feedback resistor, and the current sensitivity of the feedback coil. Both informations, the amplitude of the test signal and the feedback flux, then allow to calculate the associated SQUID parameter. Noise measurements were performed in an FLL to either the first-stage or second-stage SQUID (figures 5(b) and (c)).

## 6. SQUID characterization

### 6.1. First-stage SQUIDs

During the basic characterization of our first-stage SQUIDs at 4.2 K we measured the current sensitivities $1/M_{in}$ and $1/M_{fb}$ of the input and feedback coil, the maximum voltage swing $\Delta V_{max}$, the corresponding bias current $I_{b,max}$, as well as the normal state resistance $R_N$ of the SQUID. Based on $I_{b,max}$ we estimated the critical current $I_0$ of the Josephson junctions by using the equation [22]

$$I_0 \simeq \frac{I_{b,max}}{2} + \frac{k_B T}{2}\left(1 + \sqrt{1 + \frac{I_{b,max}}{k_B T/\Phi_0}}\right) \quad (1)$$

which is valid since the *I*–*V*-characteristic of a symmetrical SQUID can be approximated for $\Phi = n\Phi_0$ with $n$ being an integer by the *I*–*V*-characteristic of a single Josephson junction with critical current $2I_0$. Furthermore, we calculated the dynamic resistance of the SQUID by measuring the flux-to-voltage transfer coefficient $V_\Phi$ and the flux-to-current transfer coefficient $I_\Phi$ and using the relation $R_{dyn} = V_\Phi/I_\Phi$. The critical current variation $\Delta I_0$ and subsequently the screening parameter $\beta_L$ were determined either from *I*–*V*-characteristics or by directly measuring the output current swing of the SQUID in a two-stage SQUID configuration with an FLL to the second stage. Noise measurements were mainly performed in a two-stage SQUID configuration with an FLL to the first-stage SQUID. To determine the intrinsic noise of our SQUIDs, the noise contribution of the gain resistor $R_g$ used for voltage biasing as well as the noise contributions of the second-stage SQUID and the SQUID electronics were subtracted.

In total we characterized more than 20 SQUIDs that were taken from four different batches. It turned out that within a batch all SQUIDs have very similar properties, i.e. the SQUID parameters are close to identical. Because of the time consuming process we therefore characterized only a small subsample of the SQUIDs at mK temperatures. In the following we exemplary discuss the properties of SQUID w01G51SQ3 in quite some detail while the properties of the other SQUIDs are summarized in table 1.

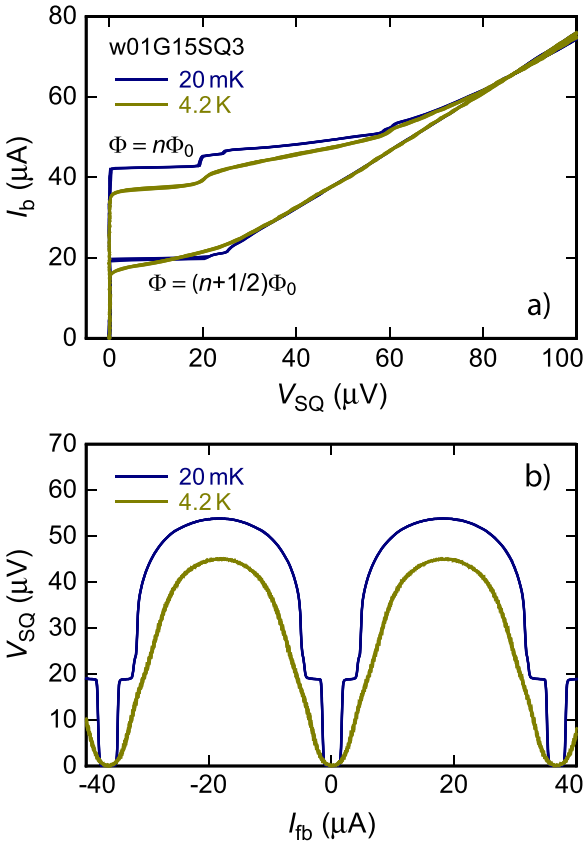


**Figure 6.** (a) *I–V*-characteristics at integer and half-integer values of applied magnetic flux $\Phi$ and (b) *V–Φ*-characteristics of SQUID w01G15SQ3 measured at 4.2 K and 20 mK in a single-stage configuration. The *V–Φ*-characteristics were taken using the bias current with maximum voltage swing.

Figure 6 shows *I–V*-characteristics and *V–Φ*-characteristics of SQUID w01G15SQ3 measured at 4.2 K and 20 mK in a single-stage configuration. At 4.2 K the SQUID is non-hysteretic and shows an almost single-junction like *I–V*-characteristic. For SQUID voltages of about 19 and 59 $\mu$V the *I–V*-characteristic shows small rounded kinks that are related to the fundamental SQUID resonance which is obviously not sufficiently damped by the washer shunts. For SQUIDs of other batches the SQUID resonance is more strongly damped due to the higher AuPd sheet resistance and therefore often not visible in the *I–V*-characteristic. The *V–Φ*-characteristic is basically sinusoidal though a deformation due to resonance effects is visible. The maximum voltage swing is $\Delta V_{\max} = 45.6\,\mu$V. From the corresponding bias current $I_{\mathrm{b,max}} = 38.4\,\mu$A we estimate a junction critical current of $I_0 = 19.5\,\mu$A using (1). This is in this case in very good agreement with the expected value of $I_0 = 19.5\,\mu$A taking into account an increase of $j_c$ of about 10% when lowering the temperature from 4.2 K to mK temperatures and assuming a target critical current density of 300 Acm$^{-2}$ for $T < 1\,K$. The critical current variation is $\Delta I_0 = 19.6\mu$A. Assuming a symmetrical SQUID with RCSJ-like junction characteristics this results in a screening parameter of $\beta_L = 0.98$ and hence a SQUID inductance of $L_s = 50.1$ pH [18] which is in good agreement with our design value. However, since the SQUID inductance is about 10% larger than numerically calculated, we expect a hysteretic SQUID behavior when lowering the operation temperature. The current sensitivities of the input and feedback coil are $1/M_{\mathrm{in}} = 12.7\,\mu\mathrm{A}/\Phi_0$ and $1/M_{\mathrm{fb}} = 36.5\,\mu\mathrm{A}/\Phi_0$ and are again very close to the numerically calculated values of 12.8 and 37.0 $\mu\mathrm{A}/\Phi_0$. The normal state resistance is $R_N = 1.5\,\Omega$ and matches the expected resistance of 1.4 $\Omega$ for this batch very well. The $I_0R_N$ product of this SQUID is 30.4 $\mu$V. The dynamic resistance $R_{\mathrm{dyn}}$ is 3.5 $\Omega$ at the positive and 4.4 $\Omega$ at the negative slope of the *V–Φ*-characteristic. Our SQUIDs are therefore slightly asymmetric. In particular, we measure a current-to-flux transfer coefficient $I_\Phi$ of 44.9 $\mu\mathrm{A}/\Phi_0$ at the positive and of 37.5 $\mu\mathrm{A}/\Phi_0$ at the negative slope. This results in an inductance asymmetry, i.e. the bias current is not entirely symmetrically injected, of about 4.5 pH.

Lowering the temperature from 4.2 K to 20 mK the critical current of the SQUID increases from 19.5 to 28.4 $\mu$A. It therefore increases more strongly than expected. The critical current variation is $\Delta I_0 = 23.7\,\mu$A resulting in a screening parameter of $\beta_L = 1.4$. For this reason and since in addition $\beta_c > 1$ the SQUID is hysteretic at mK temperatures which leads to finite voltage jumps in the *I–V*-characteristic at certain bias currents, e.g. at $I_b \simeq 42\,\mu$A. Nevertheless, the operation in a two-stage SQUID configuration with a rather high voltage bias was still possible.

For a further characterization of the SQUID, in particular for measuring the intrinsic SQUID noise and the input coil inductance $L_{\mathrm{in}}$, we built a two-stage SQUID configuration with a PTB SQUID array. We determined the first-stage SQUID input coil inductance at 4.2 K by shorting the input coil with a normal conducting bonding wire having a resistance $R_b$ in the m$\Omega$ range and measuring the current noise spectrum of this resistor. The resulting spectrum shows a low-pass filter characteristic with a white noise level that is given by $R_b$ and a cut-off frequency that is determined by $R_b$ as well as $L_{\mathrm{in}}$ and the bonding wire inductance $L_b$. By analyzing the noise spectrum we found a total circuit inductance of 1.9 nH. Assuming a wire inductance of $L_b = 300$ pH which is in accordance with our expectations and the determined wire resistance we determine an input coil inductance of 1.6 nH which is about 10% smaller compared to the numerically calculated value.

In order to allow for a quantitative analysis of the intrinsic noise of our first-stage SQUIDs we separately measured the noise spectrum of the PTB SQUID array in a single-stage configuration at mK temperatures. By fitting the acquired noise spectrum with the equation

$$S_\Phi = S_{\Phi,\mathrm{w}} + \frac{S_{\Phi,1/f}}{f^\alpha} \qquad (2)$$

we found a white noise level of $\sqrt{S_{\Phi,\mathrm{w}}} = 0.23\,\mu\Phi_0/\sqrt{\mathrm{Hz}}$ and an $1/f$ noise contribution with $\sqrt{S_{\Phi,1/f}}(1\,\mathrm{Hz}) = 4.48\,\mu\Phi_0/\sqrt{\mathrm{Hz}}$ with $\alpha = 0.9$. These noise values include the noise contribution of the SQUID electronics and were subtracted from the measured noise spectrum of the two-stage configuration with an FLL to the first-stage

**Table 1.** Summary of the SQUID characterization. While the basic SQUID parameters were determined at 4.2 K, the noise values expressed as intrinsic energy sensitivities are given for 20 mK. Because of the time consuming process, the low-temperature noise measurements were only performed for a small subsample of all tested SQUIDs.

| | $T = 4\ K$ | | | | $T = 20$ mK | | |
|---|---|---|---|---|---|---|---|
| SQUID | $I_0$ ($\mu$A) | $R_N$ ($\Omega$) | $M_{in}$ (pH) | $R_{dyn}$ ($\Omega$) | $\epsilon_w$ ($h$) | $\epsilon_{1/f}$ ($h$) | $\alpha$ |
| w01C15SQ1 | 20.1 | 1.4 | 164.3 | 1.3 | — | — | — |
| w01C15SQ4 | 20.4 | 1.4 | 164.3 | 2.0 | 4.0 | 200.3 | 0.68 |
| w01G15SQ1 | 20.3 | 1.6 | 163.0 | 1.2 | — | — | — |
| w01G15SQ3 | 19.5 | 1.5 | 163.0 | 3.5 | 4.4 | 36.3 | 0.54 |
| w02F05SQ4 | 8.7 | 2.8 | 168.3 | 2.8 | — | — | — |
| w02G05SQ4 | 10.8 | 2.5 | 165.6 | 3.5 | 2.4 | 177.2 | 0.59 |
| w02M05SQ3 | 9.8 | 2.9 | 165.6 | 4.2 | — | — | — |
| w03B15SQ3 | 8.7 | 2.3 | 168.3 | 2.4 | — | — | — |
| w03C15SQ1 | 8.6 | 2.6 | 165.6 | 3.0 | — | — | — |
| w03C15SQ4 | 10.8 | 2.4 | 165.6 | 3.2 | 2.1 | 81.1 | 0.60 |
| w03G15SQ2 | 9.7 | 2.9 | 164.3 | 2.8 | 4.7 | 36.4 | 0.54 |
| w04K05SQ1 | 8.5 | 2.6 | 165.6 | 3.4 | 1.9 | 209.5 | 0.64 |
| w04K05SQ4 | 8.9 | 1.9 | 165.6 | 1.8 | — | — | — |

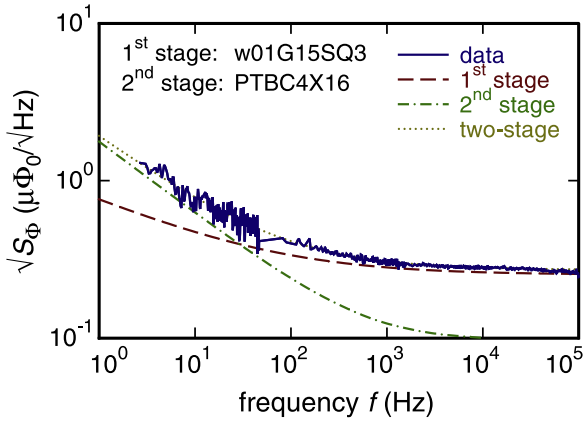


**Figure 7.** Noise spectrum $\sqrt{S_\Phi}$ of the magnetic flux noise of SQUID w01G15SQ3 measured at 20 mK in a two-stage SQUID configuration. Dashed lines represent the noise contribution of the second-stage SQUID, the intrinsic first-stage SQUID noise as well as the sum of the first- and second-stage SQUID noise.

SQUID after scaling with the measured small-signal flux gain $G_\Phi$ of the two-stage SQUID setup.

Figure 7 shows the noise spectrum of SQUID w01G15SQ3 measured at 20 mK in a two-stage SQUID configuration. By fitting the noise spectrum with (2) we determine a white noise level of $\sqrt{S_{\Phi,w}} = 0.28\ \mu\Phi_0/\sqrt{\text{Hz}}$ and an $1/f$ noise contribution with $\sqrt{S_{\Phi,1/f}}(1\text{ Hz}) = 1.89\ \mu\Phi_0/\sqrt{\text{Hz}}$ and $\alpha = 0.82$. After subtracting the SQUID array noise with the measured flux gain $G_\Phi = 2.6$ we find an intrinsic white noise level of our first-stage SQUID of $\sqrt{S_{\Phi,w}} = 0.26\ \mu\Phi_0/\sqrt{\text{Hz}}$ and an $1/f$ noise contribution with $\sqrt{S_{\Phi,1/f}}(1\text{ Hz}) = 0.75\ \mu\Phi_0/\sqrt{\text{Hz}}$ and $\alpha = 0.54$. These values correspond to intrinsic energy sensitivities of $\epsilon_w = 4.4\ h$ and $\epsilon_{1/f} = 36.3\ h$ or to coupled energy sensitivities of $\epsilon_{c,w} = 13.4\ h$ and $\epsilon_{c,1/f} = 111.3\ h$, respectively. The later values are relatively high since the magnetic coupling factor $k_{in} = 0.57$ is low as already mentioned in section 3. In terms of low-frequency noise our SQUID is competitive to the best state-of-the-art SQUIDs [11]. In particular, the noise performance of our SQUID seems not to be significantly affected by the fact that paramagnetic temperature sensors are deposited in the same sputtering system that is also used for deposition of all metal layers during SQUID fabrication (see section 4). Comparing to theory [18], the intrinsic energy sensitivity of our SQUID is about a factor of 3 higher than expected after subtracting the current noise of the washer shunts. Since a direct and independent measurement of the chip temperature of our SQUID has not been performed so far, we assumed a chip temperature of $T_{chip} \approx 200$ mK for comparison to theory. This chip temperature is our best guess after measuring the SQUID noise as a function of temperature and looking at what temperature the SQUID noise levels off. The reason for the energy sensitivity being worse is not fully clear so far. However, since the SQUID is hysteretic at 20 mK, mixing down effects due to high-frequency currents flowing inside the SQUID can not be excluded and are in turn a likely cause for the observed degradation of the energy sensitivity.

Table 1 summarizes the results of some of the SQUIDs that have been measured so far. It is obvious that within a batch the different SQUIDs show very similar results. Based on the measured critical currents $I_0$ we determine a critical current density of $j_c = 278\ \text{Acm}^{-2}$ for batch w01 and of $j_c = 117\ \text{Acm}^{-2}$ for batches w02 to w04. These values are slightly smaller compared to our design values. The normal state resistances $R_N$ somehow scatter, very likely due to inaccuracies during lithography. There is no obvious correlation between the measured noise values and the SQUID properties. However, a clear correlation between the exponent $\alpha$ and the prefactor $\epsilon_{1/f}(1\text{ Hz})$ of the $1/f$ noise exists. This can be seen in figure 8 which shows the 10 Hz $1/f$ noise component versus the exponent $\alpha$ for all SQUIDs that have been measured at mK temperatures. In addition, the figure contains data summarized in [11] being consistent with the results

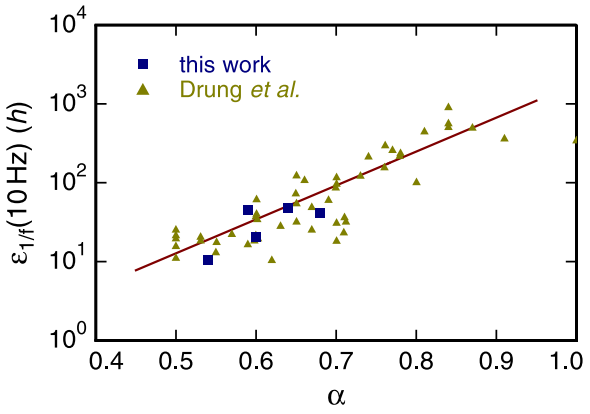


**Figure 8.** Dependence of the 10 Hz $1/f$ noise components versus the exponent $\alpha$ of the SQUIDs that were measured at mK temperatures (see table 1). For comparison, data summarized by Drung *et al* [11] are included. The dashed line is an approximation $\epsilon_{1/f}(f) \approx 0.09\,h \times (f/200\,\text{kHz})^{-\alpha}$ as given in [11].

discussed here although the devices were produced in many different facilities with quite different fabrication schemes. This might suggest that the observed correlation is perhaps universal.

### 6.2. N-SQUID series arrays

We tested a number of arrays with different number of SQUID cells. The largest arrays consist of sixteen cells. We found that the characteristic SQUID parameters such as the maximum voltage swing $\Delta V_{\text{max}}$, the normal state resistance $R_{\text{N}}$ or the dynamic resistance $R_{\text{dyn}}$ scale as expected with the number $N$ of SQUID cells. We also confirmed that the critical current $I_0$ and the current sensitivity $1/M_{\text{in}}$ of the input coil are independent off $N$. Based on the previously obtained results we selected the two most promising arrays and cooled those down to mK temperatures. In the following we exemplary discuss the properties of one SQUID (w03F13SQ9) in quite some detail and compare the results afterwards to the second array (w03L13SQ9).

Figure 9 shows $I$–$V$-characteristics and $V$–$\Phi$-characteristics of the SQUID array w03F13SQ9 measured at 4.2 K and 20 mK. At both temperatures the array is non-hysteretic and shows an almost single-junction like $I$–$V$-characteristic. However, there are some rounded kinks in the $I$–$V$-characteristic and at some voltages, e.g. at about 200 $\mu$V, the curves belonging to a magnetic flux of $n\Phi_0$ and $(n + 1/2)\Phi_0$ ($n$ is an integer) inside the SQUID loop cross each other. These features are related to the fundamental resonance of the SQUID cells that is not damped by any kind of washer shunts. However, the resonance is far away from the optimum working point so that the SQUID performance should not be degraded. This can be seen, for example, in the $V$–$\Phi$-characteristics that are almost perfectly sinusoidal. The maximum voltage swing $\Delta V_{\text{max}}$ is 119 $\mu$V at 4.2 K and 159 $\mu$V at mK temperatures. From the corresponding bias currents $I_{\text{b,max}}$ we estimate a junction critical current $I_0$ of 3.8 $\mu$A at 4.2 K and 4.3 $\mu$A at 20 mK . Taking into account that the critical current density is $j_{\text{c}} = 120\ \text{Acm}^{-2}$ at 4.2 K (see section 6.1), we find

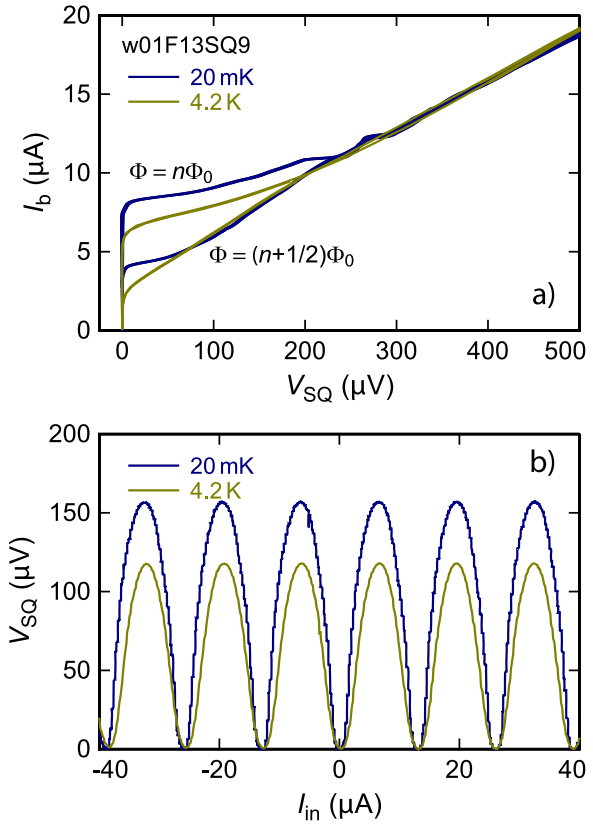


**Figure 9.** (a) $I$–$V$-characteristics at integer and half-integer values of applied magnetic flux $\Phi$ and (b) $V$–$\Phi$-characteristics of the SQUID array w03F13SQ9 measured at 4.2 K and 20 mK in a single-stage configuration. The $V$–$\Phi$-characteristics were taken using the bias current with maximum voltage swing.

a good agreement with the expected values. The critical current variation is $\Delta I_0 = 3.8\,\mu$A. Assuming a symmetrical SQUID with RCSJ-like junction characteristics this results in a screening parameter of $\beta_{\text{L}} = 0.91$ and hence a SQUID inductance of $L_{\text{s}} = 248$ pH [18]. This is about 30% larger than our numerically calculated value. The current sensitivity of the input coil is $1/M_{\text{in}} = 12.9\,\mu\text{A}/\Phi_0$ which agrees reasonable well with the calculated value of $13.8\,\mu\text{A}/\Phi_0$. The normal state resistance is $R_{\text{N}} = 54\,\Omega$ and matches the expected resistance of 58 $\Omega$ for this batch within 5%. The $I_0R_{\text{N}}$ product is 205.2 $\mu$V. The dynamic resistance $R_{\text{dyn}}$ is 40.2 $\Omega$ at the positive and 73.3 $\Omega$ at the negative slope of the $V$–$\Phi$-characteristic. Lowering the temperature to mK temperatures, these values increase of about 20% which is consistent with the increase of the maximum voltage swing. Our SQUID arrays are asymmetric as intended in the design. In particular, we measure a current-to-flux transfer coefficient $I_\Phi$ of $10.1\,\mu\text{A}/\Phi_0$ at the positive and of $5.7\,\mu\text{A}/\Phi_0$ at the negative slope. This results in an inductance asymmetry of about 88 pH which was foreseen to provide bias current feedback.

Figure 10 shows the noise spectrum of the SQUID array that was measured at 20 mK in an FLL. To determine the intrinsic noise of the array, we subtracted the noise contribution from the readout electronics. The resulting spectrum

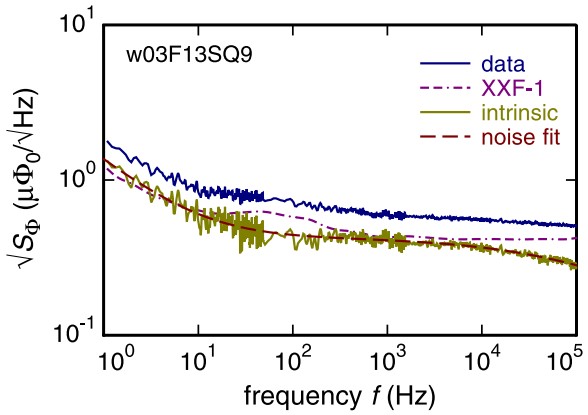


**Figure 10.** Noise spectrum $\sqrt{S_\Phi}$ of the magnetic flux noise of the SQUID array w03F13SQ9 measured at 20 mK in a single-stage SQUID configuration. Dashed lines represent the noise contribution of the SQUID electronics as well as the intrinsic noise of the SQUID array. The cut-off at high frequencies is due to the FLL bandwidth.

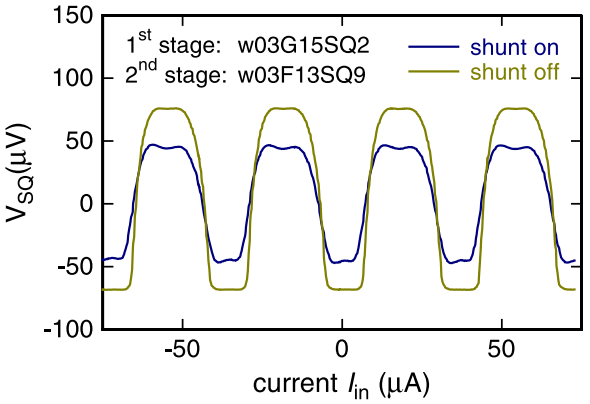


**Figure 11.** *V*–*Φ* characteristics measured at 20 mK for a two-stage SQUID configuration consisting of our first-stage SQUIDs w03G15SQ2 and the 16-SQUID series arrays w03F13SQ9. The characteristics were recorded either with or without active shunting of the preamplifier of the SQUID electronics.

of the intrinsic noise shows a slight low-pass characteristic which results from a small FLL bandwidth. By fitting the intrinsic noise spectrum using (2) we determine a white noise level of $\sqrt{S_{\Phi,\text{w}}} = 0.42\,\mu\Phi_0/\sqrt{\text{Hz}}$ and a true $1/f$ noise contribution with $\sqrt{S_{\Phi,1/f}}(1\text{ Hz}) = 1.30\,\mu\Phi_0/\sqrt{\text{Hz}}$ and $\alpha = 0.95$. These values correspond to intrinsic energy sensitivities of $\epsilon_\text{w} = 2.3\,h$ and $\epsilon_{1/f} = 22.0\,h$ or to coupled energy sensitivities of $\epsilon_{\text{c,w}} = 5.5\,h$ and $\epsilon_{\text{c},1/f} = 40.2\,h$, respectively using the numerically calculated magnetic coupling factor $k_\text{in} \simeq 0.74$. In terms of low-frequency noise this SQUID array is therefore competitive to the best state-of-the-art SQUID arrays [11]. In particular, the noise performance of the SQUID seems again not to be significantly affected by the fact that paramagnetic temperature sensors are deposited in the same sputtering system that is also used for deposition of all metal layers during SQUID fabrication (see section 4).

The properties of the second SQUID array (w03L13SQ9) are within 10% identical to the properties of w03F13SQ9. The main difference is that the critical current is about 1 $\mu$A larger compared to w03F13SQ9. For this reason, the second array is hysteretic at mK temperatures which seems to have a large negative effect on the noise performance. In particular, we determined a white noise level of $\sqrt{S_{\Phi,\text{w}}} = 0.93\,\mu\Phi_0/\sqrt{\text{Hz}}$ and a true $1/f$ noise contribution with $\sqrt{S_{\Phi,1/f}}(1\text{ Hz}) = 6.82\,\mu\Phi_0/\sqrt{\text{Hz}}$ and $\alpha = 1.04$. For both SQUID arrays we observe true $1/f$ noise with $\alpha \approx 1$. For this reason, we might observe for our SQUID arrays rather critical current than magnetic flux noise. Future measurements with bias reversal [9] will reveal if this assumption is true. It therefore seems that we may suffer from two different $1/f$ noise sources comparing our first-stage SQUIDs and the SQUID arrays.

### *6.3. Two-stage SQUID configuration*

A lumped-element two-stage SQUID configuration was set up using the first-stage SQUID w03G15SQ2 (SQ1) and the 16-SQUID series array w03F13SQ9 (SQ2). These SQUIDs were selected according to the results of the individual SQUID characterization in which they showed promising results. Both SQUIDs were mounted on separate Cu chip holders and were connected with superconducting NbTi wires. In contrast to the SQUIDs these wires were not shielded against external interferences and therefore against noise pickup. For this reason, discrete noise peaks were observed in the noise spectra that were removed by a simple peak detection algorithm during the data analysis. A metal thin-film resistor with $R_\text{g} = 600\text{ m}\Omega$ was inserted in one of the wires connecting both SQUIDs to provide a voltage bias for SQ1. The two-stage SQUID setup was mounted on the mixing chamber of a dilution refrigerator and cooled down to 20 mK . During most of the measurements, in particular during the noise measurements, the preamplifier of the SQUID electronics was actively shunted [13].

Figure 11 shows *V*–*Φ*-characteristics of our two-stage SQUID configuration that were measured both with and without active shunting of the preamplifier of the SQUID electronics. The characteristics show a tiny double-dip since the output current of SQ1 modulates SQ2 by about 54% of a flux quantum which is slightly larger than the flux difference between the maximum and minimum of the SQ2 *V*–*Φ*-characteristic at the positive slope. However, there are unique working points allowing for stable SQUID operation in an FLL without the unfavorable possibility for locking to multiple working points. The flux-to-voltage and flux-to-current transfer coefficients of the two-stage SQUID configuration are $V_\Phi = 1.39\text{ mV}/\Phi_0$ and $I_\Phi = 23.6\,\mu\text{A}/\Phi_0$. The dynamic resistance is $R_\text{dyn} = 59\,\Omega$. The small signal flux gain is $G_\Phi = 1.76$ meaning that there is in fact flux gain between SQ1 and SQ2. Taking into account the measured noise spectra of both type of SQUIDs we expect the noise spectrum of the two-stage SQUID configuration to be dominated by the $1/f$ noise of SQ1 for frequencies $f \leqslant 1$ kHz and by the white noise of SQ2 for $f \geqslant 1$ kHz. It turns out that the number of SQUIDs is not sufficient to reduce the second-stage SQUID noise to a negligible level as originally intended. However, the flux-to-voltage transfer coefficient $V_\Phi$ of our SQUID

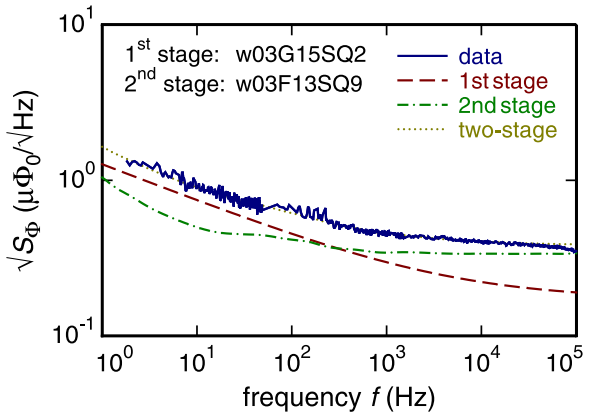


**Figure 12.** Magnetic flux noise $\sqrt{S_\Phi}$ versus frequency $f$ that was measured at 20 mK for our two-stage SQUID configuration. Data are smoothened by removing noise peaks with a simple peak detection algorithm. Dashed and dashed-dotted lines indicate different noise contributions while the dotted line is a fit to the data.

arrays can in future be easily enhanced either by using higher ohmic shunt resistors for junction shunting or by using SQUID arrays with a larger number of SQUID cells. Both is planned to be included in our next design.

Due to the needlessly long NbTi wires between the first- and second-stage SQUID (the SQUIDs were not mounted very close to each other), the cable delay $t_d$ between the FLL electronics and the first-stage SQUID takes rather large values. This prohibited the measurement of the ultimate bandwidth of the two-stage SQUID configuration which finally determines the detector rise time [9]. With this rather large value of $t_d$ we achieved a stable FLL operation with a bandwidth of several 100 kHz . Even though this bandwidth is not yet sufficient for resolving an intrinsic detector rise time below 100 ns, we expect to be able to reduce the cable delay significantly (ultimately by fabricating both SQUIDs on the same chip) and therefore to increase the system bandwidth considerably. In particular, the total SQUID gain $G_S = V_\Phi M_{fb}/R_{fb}$ which is given by the flux-to-voltage transfer coefficient $V_\Phi$, the current sensitivity $M_{fb}$ of the feedback coil of the first-stage SQUID and the feedback resistor $R_{fb}$ [9] is comparable to state-of-the-art SQUIDs which we routinely operate with system bandwidths of up to 10 MHz.

Figure 12 shows a noise spectrum of the two-stage SQUID configuration that was measured at 20 mK. The white noise level is $\sqrt{S_{\Phi,w}} = 0.37\,\mu\Phi_0/\sqrt{\text{Hz}}$ and the value of the $1/f$ noise contribution is $\sqrt{S_{\Phi,1/f}}(1\text{ Hz}) = 1.46\,\mu\Phi_0/\sqrt{\text{Hz}}$ with $\alpha = 0.48$. As expected the noise of SQ2 dominates the two-stage noise spectrum for frequencies $f > 1$ kHz while the noise of SQ1 dominates for $f < 1$ kHz . The current noise of the gain resistor $R_g$ is negligible since the sum of the dynamic resistance of SQ1 and the gain resistor is larger than 1 $\Omega$ and the resulting flux noise is hence well below $0.1\,\mu\Phi_0/\sqrt{\text{Hz}}$. Using the current sensitivity of the input coil and the input coil inductance of SQ1 we get coupled energy sensitivity values of $\epsilon_{c,w} = 27.1\,h$ and $\epsilon_{c,1/f}(1\text{ Hz}) = 421.7\,h$. The $1/f$ noise contribution of the two-stage SQUID setup is hence very low and is similar to the best SQUIDs we typically use for the readout of our detectors. For the reasons mentioned above, the white noise contribution is about a factor of 2 higher compared to state-of-the-art two-stage SQUID configurations. However, taking into account that the magnetic coupling factor between the input coil and the SQUID loop of SQ1 is low and that there are rather large parasitic inductances in the SQ1 input circuit (see section 3), we expect an energy sensitivity of about $\epsilon_{c,w} = 10\,h$ and $\epsilon_{c,1/f} = 150\,h$ for a future SQUID design that is optimized in terms of magnetic coupling and parasitic inductances. Nevertheless, the present two-stage SQUID configuration already allows for the readout of high-resolution detectors with $\Delta E_{FWHM} \simeq 1.5$ eV, thus fully matching our design goals.

## 7. Conclusion

We have analyzed the influence of the coupled energy sensitivity $\epsilon_c(f)$ of a SQUID on the achievable energy resolution $\Delta E_{FWHM}$ of MMCs. We have found that the readout of high-resolution detectors with sub-eV energy resolution requires a SQUID readout with $\epsilon_{c,w} < 15\,h$, an $1/f$ corner frequency $f_c < 200$ Hz and a SQUID input coil inductance of about $L_{in} \simeq 900$ pH assuming true $1/f$ noise. Furthermore, we have developed two dc-SQUID designs, namely a first-stage SQUID as well as a $N$-SQUID series array, that are suited for the readout of high-resolution MMCs. We have fabricated four different batches and have shown that the properties of fabricated SQUIDs are in good agreement with our design values. Our first-stage SQUIDs show an intrinsic energy sensitivity as low as $\epsilon_w = 2\,h$ in the white noise region and an $1/f$ noise contribution with a prefactor $\epsilon_{1/f}(1\text{ Hz})$ as low as $36\,h$. The coupled energy resolution suffers from a relatively small magnetic coupling factor $k_{in}$ which mainly results from large parasitic inductances in the SQUID input circuit. We observed a correlation between the $1/f$ noise exponent $\alpha$ and the prefactor $\epsilon_{1/f}(1\text{ Hz})$ similar to the one reported in [11]. The properties of fabricated $N$-SQUID series arrays scale as expected with the number of SQUID cells. The coupled energy sensitivity is below $6\,h$ in the white noise region and has a prefactor $\epsilon_{1/f}(1\text{ Hz})$ of the true $1/f$ noise contribution of about $40\,h$. Using one of our first-stage SQUIDs as well as one of our 16-SQUID series arrays we have built a two-stage SQUID configuration with a coupled energy sensitivity of $\epsilon_{c,w} = 27\,h$ and $\epsilon_{c,1/f}(1\text{ Hz}) = 421\,h$. With this setup reading out an optimized MMC we should already be able to reach an energy resolution of $\Delta E_{FWHM} = 1.5$ eV, thus fully matching our design goals. With the improvements discussed above it should moreover be possible to read out state-of-the-art MMC detectors with sub-eV energy resolution.

## Acknowledgments

We would like to thank J Beyer, D Drung and T Schurig for many fruitful and stimulating discussions and providing SQUID arrays for characterization of our first-stage SQUIDs.

Furthermore, we are very grateful to V Schultheiss and T Wolf for technical support during SQUID fabrication. This work was partially supported by the European Community Research Infrastructures under the FP7 Capacities Specific Programme, MICROKELVIN project number 228464.

## References

[1] Clarke J and Braginski A I (ed) 2004 *The SQUID Handbook: Fundamentals and Technology of SQUIDs and SQUID Systems Weinheim* (New York: Wiley)
[2] Irwin K D and Hilton G C 2005 Transition-edge sensors *Cryogenic Particle Detection* (*Topics in Applied Physics* vol 99) ed C Enss (Berlin: Springer) pp 63–149
[3] Bandler S R, Irwin K D, Kelly D, Nagler P N, Porst J-P, Rotzinger H, Sadleir J E, Seidel G M, Smith S J and Stevenson T R 2012 Magnetically Coupled Microcalorimeters *J. Low Temp. Phys.* **167** 254–68
[4] Fleischmann A, Enss C and Seidel G M 2005 Metallic magnetic calorimeters *Cryogenic Particle Detection* (*Topics in Applied Physics* vol 99) ed C Enss (Berlin: Springer) pp 151–216
[5] Fleischmann A *et al* 2009 Metallic magnetic calorimeters *AIP Conf. Proc.* **1185** 571–8
[6] Fleischmann A *et al* 2014 in preparation
[7] Enss C, Fleischmann A, Horst K, Schönefeld J, Sollner J, Adams J S, Huang Y H, Kim Y H and Seidel G M 2000 Metallic magnetic calorimeters for particle detection *J. Low Temp. Phys.* **121** 137–76
[8] Rotzinger H, Adams J, Bandler S R, Beyer J, Eguchi H, Figueroa-Feliciano E, Hsieh W, Seidel G M and Stevenson T 2008 Performance of micro-fabricated magnetic calorimeters arrays for x-ray spectroscopy *J. Low Temp. Phys.* **151** 351–6
[9] Drung D and Mück M 2004 SQUID electronics *The SQUID Handbook: Fundamentals and Technology of SQUIDs and SQUID Systems* ed J Clarke and A I Braginski (Weinheim: Wiley)
[10] Drung D, Assmann C, Beyer J, Kirste A, Peters M, Ruede F and Schurig T 2007 Highly sensitive and easy-to-use SQUID sensors *IEEE Trans. Appl. Supercond.* **17** 699–704
[11] Drung D, Beyer J, Storm J-H, Peters M and Schurig T 2011 Investigation of low-frequency excess flux noise in dc SQUIDs at mK temperatures *IEEE Trans. Appl. Supercond.* **21** 340–4
[12] McCammon D 2005 Thermal equilibrium detectors-an introduction *Cryogenic Particle Detection* (*Topics in Applied Physics* vol 99) ed C Enss (Berlin: Springer)
[13] Drung D, Hinnrichs C and Barthelmess H 2006 Low-noise ultra-high-speed dc SQUID readout electronics *Supercond. Sci. Technol.* **19** S235–41
[14] Ruede F 2008 Hochempfindliche stromsensoren auf dc-SQUID-basis für den betrieb in elektro-magnetisch gestörter umgebung *PhD Thesis* Technische Universität, Berlin
[15] Anton S M *et al* 2013 Magnetic flux noise in dc SQUIDs: temperature and geometry dependence *Phys. Rev. Lett.* **110** 147002
[16] Fourie C J and Perold W J 2005 Simulated inductance variations in RSFQ circuit structures *IEEE Trans. Appl. Supercond.* **15** 300–3
[17] Kamon M, Tshuk J and White J K 1994 FASTHENRY: a multipole-accelerated 3D inductance extraction program *IEEE Trans. Microw. Theory Tech.* **42** 1750–8
[18] Tesche C D and Clarke J 1977 DC SQUID: noise and optimization *J. Low Temp. Phys.* **29** 301–31
[19] Wellstood F C, Urbina C and Clarke J 1994 Hot-electron effects in metals *Phys. Rev.* B **49** 5942–55
[20] Uehara G, Matsuda M, Kazami K, Takada Y and Kado H 1993 Asymmetric bias injection technique for drung-type superconducting quantum interference devices *Japan. J. Appl. Phys.* **32** L1735–8
[21] Kempf S, Ferring A, Fleischmann A, Gastaldo L and Enss C 2013 Characterization of the reliability and uniformity of an anodization-free fabrication process for high-quality Nb/Al-$AlO_x$/Nb Josephson junctions *Supercond. Sci. Technol.* **26** 065012
[22] Drung D *et al* 1996 Integrated $YBa_2Cu_3O_{7-x}$ magnetometer for biomagnetic measurements *Appl. Phys. Lett.* **68** 1421–3